XLI CILAMCE
XLI Ibero-Latin American Congress on Computational Methods in Engineering
16-19 November, 2020 FOZ DO IGUAÇU PARANÁ - BRAZIL

A finite strain non-isothermal phase-field model for damage and fracture in elasto-plastic impact problem

G.A. Haveroth[1], A.P.C. Dias[2], M.L. Bittencourt[2], J.L. Boldrini[2]

[1]*Department of Applied Mathematics, Institute of Mathematics, Statistics and Scientific Computing, University of Campinas*
Praça Sergio Buarque de Holanda, 651. Cidade Universitária, zip code 13083-859, Campinas-SP, Brazil
geovaneah@gmail.com
[2]*Department of Integrated Systems, School of Mechanical Engineering, University of Campinas*
Mendeleyev, 200. Cidade Universitária, zip code 13083-860, Campinas-SP, Brazil
diasfem@gmail.com, *mlb@fem.unicamp.br*, *josephbold@gmail.com*

Abstract. This paper presents a thermodynamically consistent non-isothermal phase-field framework to model the damage and fracture effects in elasto-plastic materials under finite strain. Following Boldrini *et al.* [1], the adopted methodology is based on the use of the principle of virtual power, energy balance, and the second law of thermodynamics in the form of a Clausius-Duhem inequality for entropy. Contact constraints are introduced conveniently in the weak form of the resulting motion equation. A frictionless impact fracture problem simulation, disregarding thermal effects, shows that the proposed model can reproduce qualitatively the crack initialization and subsequent propagation.

Keywords: Non-linear structural mechanics, Damage, Fracture, Phase-field, Plasticity, Contact mechanics, Impact

1 Introduction

Understanding damage and fracture phenomena can lead to improved design of components and also improve inspection, maintenance, and renewal policies for existing and future infrastructure in several fields. In this concern, the use of phase-field methodology is a sound alternative to the classical strategies for damage and fracture modeling, as evidenced by the number of publications on the subject in recent years [1–7]. This methodology overcomes the main difficulties associated with the initiation and subsequent crack propagation, especially when they occur in complex geometries. Moreover, its diffuse approximation of discontinuities avoids the need to remeshing along the crack propagation [8].

Miehe *et al.* [2, 9] developed a phase-field variational formulation for crack propagation in brittle elastic solids. This is the principal study (not the pioneer) concerning phase-field modeling for the description of cracks. Several numerical examples were performed, showing the potentiality of this methodology. Based on the Miehe's methodology, several studies with contributions for this theme were developed [4, 5, 10, 11]. In particular, Boldrini *et al.* [1] developed a thermodynamically consistent non-isothermal phase-field model for brittle crack description based on the principle of virtual power, balance energy, and the second law of thermodynamics. The resulting model showed generality, recovering the Miehe's based models by adopting convenient simplifying hypotheses. Also based on Miehe's study, Ulmer *et al.* [12] outlined a phase-field model for ductile fracture description. Following the previous studies, several enrichments concerning physical hypotheses, degradation functions, and how these functions affect the free-energies were presented [6, 7, 13].

Although there are many works about damage in impact problems in the literature [14–18], numerical phase-field models applicable to general cases considering the damage and fracture evolutions in impact problems with elasto-plastic material remain under development as can be seen in [19, 20]. Franke *et al.* [19], presented a variational contact algorithm applied to a phase-field fracture approach for a contact problem considering finite strain. While Hesch *et al.* [20] expanded the previous formulation proposing a contact algorithm applied to a phase-field approach to brittle fracture. Both papers show that phase-field approaches allow for the numerical simulation of complex fracture problems, as bodies arise in contact and impact situations.

In this study, we present a general thermodynamically consistent non-isothermal phase-field model for evo-

lution of damage and fracture. This model is written in Lagrangian coordinates and developed for elasto-plastic materials under hypothesis of finite strain. In addition, we also consider the contact, disregarding friction effects, by the imposition of classical constraints in the boundary of the bodies.

2 Fundamental laws in Lagrangian Coordinates for the Damage Phase-field Model

Let us consider the usual regularity hypothesis of continuum mechanics and assume a body that at time $t = 0$ occupies a configuration $\mathcal{B}_0 \subset \mathbb{R}^3$ with Lagrangian coordinates $\boldsymbol{p}$ and $\mathcal{D}_0$ denotes an arbitrary regular sub-domain of $\mathcal{B}_0$. In this study, we assume that the damage phase-field $\varphi = \varphi(\boldsymbol{p}, t)$ (written in Lagrangian coordinates $\boldsymbol{p}$) is a dynamic variable, and its governing equation is obtained from the principle of virtual power (PVP). Moreover, we adopt the multiplicative decomposition of the deformation gradient $\boldsymbol{F}$ tensor as

$$\boldsymbol{F} = \boldsymbol{F}^e \boldsymbol{F}^p \boldsymbol{F}^\theta, \tag{1}$$

where $\boldsymbol{F}^e$, $\boldsymbol{F}^p$ and $\boldsymbol{F}^\theta$ are, respectively, the elastic, plastic and thermal deformation gradient [21].

The first physical law to be considered is the conservation of mass. It is expressed by the continuity equation for the material density $\rho_0 = \rho_0(\boldsymbol{p})$ of the reference configuration as

$$\dot{\rho_0} = 0. \tag{2}$$

The dynamic equations are obtained following the same methodology described in Boldrini *et al.* [1] and Haveroth *et al.* [7]. This derivation uses the PVP considering several kinds of forces resulting in the expressions

$$\begin{cases} \rho_0 \dot{\boldsymbol{v}} = \mathrm{div}_p(\boldsymbol{FS}) + \rho_0 \boldsymbol{f}_0 & \text{in } \mathcal{D}_0 \\ \boldsymbol{P}\boldsymbol{n}_0 = \boldsymbol{t}_0 & \text{in } \partial\mathcal{D}_0 \end{cases} \quad \text{and} \quad \begin{cases} 0 = \mathrm{div}_p(\boldsymbol{h}_0) - b_0 & \text{in } \mathcal{D}_0 \\ \boldsymbol{h}_0 \cdot \boldsymbol{n}_0 = t_{\boldsymbol{h}0} & \text{in } \partial\mathcal{D}_0 \end{cases}. \tag{3-4}$$

Herein, $\boldsymbol{S}$ the second Piola-Kirchhoff stress tensor, $\boldsymbol{P} = \boldsymbol{FS}$ is the first Piola-Kirchhorff stress tensor, $\boldsymbol{f}_0$ is the specific body force vector, $\boldsymbol{n}_0$ is the unitary external normal to $\mathcal{D}_0$, the (vectorial) microstress $\boldsymbol{h}_0$, a (scalar) microforce b_0 and the contact microforce by unit of area $t_{\boldsymbol{h}0}$. Equation (3) is the conventional linear balance equation associated to the macroscopic equilibrium, while (4) may be considered a microbalance equation associated with the phase-field [9].

The first principle of the thermodynamics postulates the balance of energy in the system. It can be expressed by the following local form

$$\rho_0 \dot{e}_0 = -\mathrm{div}_p(\boldsymbol{q}_0) + \rho_0 r_0 + \frac{1}{2}\boldsymbol{S} : \dot{\boldsymbol{C}} + b_0 \dot{\varphi} + \boldsymbol{h}_0 \cdot \nabla_p \dot{\varphi}, \tag{5}$$

where e_0 is the specific internal density, $\boldsymbol{q}_0$ is the heat flux vector in the Lagrangian configuration, r_0 is the specific heat source/sink density and $\boldsymbol{C} = \boldsymbol{F}^T\boldsymbol{F}$ is the right Cauchy-Green strain tensor.

Based in the arguments presented in [1, 22], the second principle of thermodynamics is given in a Clausius-Duhem differential form by

$$\rho_0 \dot{\eta}_0 \geq -\mathrm{div}\left(\frac{\boldsymbol{q}_0}{\theta}\right) + \rho_0\left(\frac{r_0}{\theta}\right) \quad \text{in } \mathcal{D}_0, \tag{6}$$

where η_0 is the specific entropy density, $\theta > 0$ the absolute temperature and r_0/θ is the specific entropy production associated to the heat generation.

In summary, equations (2-6) define the basic governing system of equations of the developed phase-field model. They give rise to the initial-boundary value problem (IBVP) wherewith we want to find on $\mathcal{B}_0$, at time t, the displacement $\boldsymbol{u}$ and velocity $\boldsymbol{v}$ fields, the phase-field φ and the specific internal energy e_0 according to

$$\begin{cases} \dot{\rho_0} = 0, \\ \dot{\boldsymbol{u}} = \boldsymbol{v}, \\ \rho_0 \dot{\boldsymbol{v}} = \mathrm{div}_p(\boldsymbol{FS}) + \rho_0 \boldsymbol{f}_0, \\ 0 = \mathrm{div}_p(\boldsymbol{h}_0) - b_0 + \rho_0 a_0, \\ \rho_0 \dot{e_0} = -\mathrm{div}_p(\boldsymbol{q}_0) + \rho_0 r_0 + \frac{1}{2}\boldsymbol{S} : \dot{\boldsymbol{C}} + b_0 \dot{\varphi} + \boldsymbol{h}_0 \cdot \nabla_p \dot{\varphi}, \end{cases} \tag{7}$$

given the body force vector field $\boldsymbol{f}_0$, the specific density of energy a_0 and the specific heat source/sink density r_0. We also consider that the entropy inequality (6) must be ensured. The boundary and initial conditions of this problem are given, respectively, by

$$\left\{\begin{array}{lll} \boldsymbol{u}=\boldsymbol{0} & \text{on} & \partial\mathcal{B}_t^{D_0} \\ \boldsymbol{u}=\bar{\boldsymbol{u}} & \text{on} & \partial\mathcal{B}_t^{D_u} \\ \boldsymbol{P}\boldsymbol{n}_0=\boldsymbol{t}_0 & \text{on} & \partial\mathcal{B}_t^{N_\sigma} \\ \boldsymbol{h}_0\cdot\boldsymbol{n}_0=t_{\boldsymbol{h}0} & \text{on} & \partial\mathcal{B}_t^{N_h} \end{array}\right. \quad \text{and} \quad \left\{\begin{array}{l} \rho=\rho(\boldsymbol{p}) \\ \boldsymbol{v}=\boldsymbol{v}(\boldsymbol{p}) \\ \dot{\boldsymbol{v}}=\dot{\boldsymbol{v}}(\boldsymbol{p}) \quad \text{in} \quad \mathcal{B}_0 \ \text{at} \ t=0 \\ \varphi=\varphi(\boldsymbol{p}) \\ e_0=e_0(\boldsymbol{p}) \end{array}\right. , \tag{8-9}$$

where $\boldsymbol{u}=\boldsymbol{0}$ and $\boldsymbol{u}=\bar{\boldsymbol{u}}\neq\boldsymbol{0}$ denotes the prescribed displacements on the Dirichlet boundaries, $\boldsymbol{t}$ and $t_{\boldsymbol{h}0}$ denotes, respectively, the macro and micro-traction prescribed on the Neumann boundaries. These boundaries are such that $\mathcal{B}_t^{D_0}\cup\partial\mathcal{B}_t^{D_u}\cup\partial\mathcal{B}_t^{N_\sigma}=\partial\mathcal{B}_t$ and $\mathcal{B}_t^{D_0}\cap\partial\mathcal{B}_t^{D_u}\cap\partial\mathcal{B}_t^{N_\sigma}=\emptyset$.

The second Piola-Kirchhoff stress tensor $\boldsymbol{S}$, the volumetric density of energy b_0, the flux of energy $\boldsymbol{h}_0$ and the heat flux vector field $\boldsymbol{q}_0$ are quantities, whose expressions are constitutive relations obtained by thermodynamical consistency by satisfying (6). The constitutive relations are depending on the $\boldsymbol{u}$, $\boldsymbol{v}$, φ and e_0 fields. The absolute temperature θ can be obtained from the specific internal energy e_0 and the specific Helmholtz free-energy potential.

3 Constitutive relations

Let us obtain the thermodynamic consistent constitutive relations. By using the balance of energy (5), the entropy inequality (6) can be expressed in terms of the specific Helmholtz free-energy $\psi=e_0-\theta\eta_0$ by

$$0\leq-\rho_0\left(\dot{\psi}+\eta_0\dot{\theta}\right)+\frac{1}{2}\boldsymbol{S}:\dot{\boldsymbol{C}}+b_0\dot{\varphi}+\boldsymbol{h}_0\cdot\nabla_p\dot{\varphi}-\frac{1}{\theta}\boldsymbol{q}_0\cdot\nabla_p\theta. \tag{10}$$

Also, consider the specific free-energy given according to

$$\psi=\psi\left(\Gamma_0\right) \quad \text{with} \quad \Gamma_0=\left\{\theta,\varphi,\nabla_p\theta,\nabla_p\varphi,\boldsymbol{C},\boldsymbol{C}^p,\boldsymbol{\alpha}\right\}, \tag{11-12}$$

where $\boldsymbol{C}^p=\boldsymbol{F}^{pT}\boldsymbol{F}^p$ is the plastic right Cauchy-Green strain tensor, and $\boldsymbol{\alpha}$ denotes the hardening variable set. Based on Boldrini *et al.* [1], the terms $\boldsymbol{S}$, b_0, $\boldsymbol{h}_0$ and $\boldsymbol{q}_0$ are decomposed in their reversible (non-dissipative) and irreversible (dissipative) parts. Therefore, its is assumed that

$$\boldsymbol{S}=\boldsymbol{S}^{(r)}+\boldsymbol{S}^{(ir)}, \quad b_0=b_0^{(r)}+b_0^{(ir)}, \quad \boldsymbol{h}_0=\boldsymbol{h}_0^{(r)}+\boldsymbol{h}_0^{(ir)} \quad \text{and} \quad \boldsymbol{q}_0=\boldsymbol{q}_0^{(r)}+\boldsymbol{q}_0^{(ir)}, \tag{13-16}$$

where $\boldsymbol{S}^{(r)}$ and $\boldsymbol{S}^{(ir)}$ are symmetric tensors. These expressions must be found in order that the entropy condition be valid for any admissible process. They can be obtained by replacing the time derivative of ψ into the entropy condition ans considering (13-16) as

$$\begin{aligned} 0 \quad \leq \quad & -\rho_0\left(\eta_0+\partial_\theta\psi\right)\dot{\theta}+\left(b_0^{(r)}-\rho_0\partial_\varphi\psi\right)\dot{\varphi}-\rho_0\partial_{\nabla_p\theta}\psi\cdot\nabla_p\dot{\theta}-\left(\rho_0\partial_{\nabla_p\varphi}-\boldsymbol{h}_0^{(r)}\right)\cdot\nabla_p\dot{\varphi} \\ & +\left(\frac{1}{2}\boldsymbol{S}^{(r)}-\rho_0\partial_{\boldsymbol{C}}\psi\right):\dot{\boldsymbol{C}}-\frac{1}{\theta}\boldsymbol{q}_0^{(r)}\cdot\nabla_p\theta+\boldsymbol{h}_0^{(ir)}\cdot\nabla_p\dot{\varphi}+b_0^{(ir)}\dot{\varphi}+\frac{1}{2}\boldsymbol{S}^{(ir)}:\dot{\boldsymbol{C}} \\ & -\rho_0\partial_{\boldsymbol{C}^p}\psi:\dot{\boldsymbol{C}}^p-\rho_0\partial_{\boldsymbol{\alpha}}\psi\cdot\dot{\boldsymbol{\alpha}}-\frac{1}{\theta}\boldsymbol{q}_0^{(ir)}\cdot\nabla_p\theta. \end{aligned} \tag{17}$$

The reversible terms of the inequality (17) must be chosen such that for any admissible process there is no entropy increase, that is,

$$\begin{aligned} 0 \quad = \quad & -\rho_0\left(\eta_0+\partial_\theta\psi\right)\dot{\theta}+\left(b_0^{(r)}-\rho_0\partial_\varphi\psi\right)\dot{\varphi}-\rho_0\partial_{\nabla_p\theta}\psi\cdot\nabla_p\dot{\theta}-\left(\rho_0\partial_{\nabla_p\varphi}-\boldsymbol{h}_0^{(r)}\right)\cdot\nabla_p\dot{\varphi} \\ & +\left(\frac{1}{2}\boldsymbol{S}^{(r)}-\rho_0\partial_{\boldsymbol{C}}\psi\right):\dot{\boldsymbol{C}}-\frac{1}{\theta}\boldsymbol{q}_0^{(r)}\cdot\nabla_p\theta. \end{aligned} \tag{18}$$

This equality can be obtained taking each additive term as zero. Once the quantities $\dot{\theta}$, $\dot{\varphi}$, $\nabla_p\dot{\theta}$, $\nabla_p\dot{\varphi}$, $\dot{\boldsymbol{C}}$ and $\nabla_p\theta$ can be given as arbitrary values, their respective coefficients must be zero. Then, in order to (18) holds, we must have

$$\partial_{\nabla_p\theta}\psi=\boldsymbol{0} \quad \text{and} \quad \eta_0=-\partial_\theta\psi, \tag{19}$$

and the reversible parts of $\boldsymbol{S}$, b_0, $\boldsymbol{h}_0$ and $\boldsymbol{q}_0$ are given, respectively, by

$$\boldsymbol{S}^{(r)} = 2\rho_0 \partial_{\boldsymbol{C}} \psi, \quad b_0^{(r)} = \rho_0 \partial_{\varphi} \psi, \quad \boldsymbol{h}_0^{(r)} = \rho_0 \partial_{\nabla_p \varphi} \psi \quad \text{and} \quad \boldsymbol{q}_0^{(r)} = \boldsymbol{0}. \tag{20-23}$$

Note that due to (19), the arguments of ψ may be restarted as

$$\psi = \psi\left(\tilde{\Gamma}_0\right) \quad \text{with} \quad \tilde{\Gamma}_0 = \left\{\theta, \varphi, \nabla_p \varphi, \boldsymbol{C}, \boldsymbol{C}^p, \boldsymbol{\alpha}\right\}. \tag{24}$$

The remaining terms of (18), the irreversible terms, are given by

$$0 \leq \boldsymbol{h}_0^{(ir)} \cdot \nabla_p \dot{\varphi} + b_0^{(ir)} \dot{\varphi} + \frac{1}{2} \boldsymbol{S}^{(ir)} : \dot{\boldsymbol{C}} - \rho_0 \partial_{\boldsymbol{C}^p} \psi : \dot{\boldsymbol{C}}^p - \rho_0 \partial_{\boldsymbol{\alpha}} \psi \cdot \dot{\boldsymbol{\alpha}} - \frac{1}{\theta} \boldsymbol{q}_0^{(ir)} \cdot \nabla_p \theta. \tag{25}$$

The positiveness of (25) is imposed by requiring separate positiveness of the non-plastic, and plastic processes:

$$0 \leq \boldsymbol{h}_0^{(ir)} \cdot \nabla_p \dot{\varphi} + b_0^{(ir)} \dot{\varphi} + \frac{1}{2} \boldsymbol{S}^{(ir)} : \dot{\boldsymbol{C}} - \frac{1}{\theta} \boldsymbol{q}_0^{(ir)} \cdot \nabla_p \theta, \tag{26}$$

$$0 \leq -\rho_0 \partial_{\boldsymbol{C}^p} \psi : \dot{\boldsymbol{C}}^p - \rho_0 \partial_{\boldsymbol{\alpha}} \psi \cdot \dot{\boldsymbol{\alpha}}. \tag{27}$$

In next sections, the concept of pseudo potential of dissipation is used in order to satisfy the first inequality. The second one will be satisfied by using the principle of maximum plastic dissipation. Moreover, for the sake of simplicity, as in Frémond [23, p.27], we assume that the flux term $\boldsymbol{h}_0$ is purely reversible, that is, $\boldsymbol{h}_0^{(ir)} = \boldsymbol{0}$, obtaining

$$\boldsymbol{h}_0 = \boldsymbol{h}_0^{(r)} = \rho_0 \partial_{\nabla_p \varphi} \psi. \tag{28}$$

3.1 Non-plastic dissipation

In order to satisfy the inequality (26), the concept of non-plastic pseudo-potential of dissipation is employed. It is given by the functional

$$\psi_d^n = \psi_d^n\left(\dot{\varphi}, \dot{\boldsymbol{C}}, \nabla_p \theta, \tilde{\Gamma}_0\right), \tag{29}$$

such that $\psi_d^n(\cdot) \geq 0$ for all $\left\{\dot{\varphi}, \dot{\boldsymbol{C}}, \nabla_p \theta, \tilde{\Gamma}_0\right\}$, $\psi_d\left(0, \boldsymbol{0}, \boldsymbol{0}, \tilde{\Gamma}_0\right) = 0$ and is continuous and convex with respect to the variables $\left\{\dot{\varphi}, \dot{\boldsymbol{C}}, \nabla_p \theta\right\}$. In particular, when ψ_d^n is differentiable, it is enough to take $b_0^{(ir)}$, $\boldsymbol{S}^{(ir)}/2$ and $-\boldsymbol{q}_0^{(ir)}/\theta$, as the subdifferential of $\psi_d^n(\cdot)$ respectively with respect to $\dot{\varphi}$, $\dot{\boldsymbol{C}}$ and $\nabla_p \theta$. Therefore,

$$\partial_{\dot{\varphi}} \psi_d^n = b_0^{(ir)}, \quad \partial_{\dot{\boldsymbol{C}}} \psi_d^n = \frac{1}{2} \boldsymbol{S}^{(ir)} \quad \text{and} \quad \partial_{\nabla_p \theta} \psi_d^n = -\frac{1}{\theta} \boldsymbol{q}^{(ir)}. \tag{30-32}$$

By using the previous results and from (13-16) and (20-23), the final expressions for $\boldsymbol{S}$, b_0 and $\boldsymbol{q}_0$ are, respectively,

$$\boldsymbol{S} = 2\rho_0 \partial_{\boldsymbol{C}} \psi + 2\partial_{\dot{\boldsymbol{C}}} \psi_d^n, \quad b_0 = \rho_0 \partial_{\varphi} \psi + \partial_{\dot{\varphi}} \psi_d^n \quad \text{and} \quad \boldsymbol{q}_0 = -\theta \partial_{\nabla_p \theta} \psi_d^n. \tag{33-35}$$

3.2 Plastic dissipation: plastic flow rule and hardening law

The inequality (27) is satisfied based on the arguments of Simo [24], which considers the principle of maximum plastic dissipation, and adopts an uncoupled free-energy density function (24) in relation to the internal variables set $\boldsymbol{\alpha}$ as

$$\psi = \bar{g}\bar{\psi}\left(\boldsymbol{C}, \boldsymbol{C}^p, \hat{\Gamma}_0\right) + \tilde{\psi}\left(\boldsymbol{\alpha}, \hat{\Gamma}_0\right) \quad \text{with} \quad \hat{\Gamma}_0 = \left\{\theta, \varphi, \nabla_p \varphi\right\}. \tag{36}$$

Here, we assume that the degraded state of the material, described by the scalar function $\bar{g} = g(\varphi)$, remains unchanged in the plastic dissipation process.

By applying similar arguments of Simo (details can be found in Haveroth [25, pg.85]), the flow rule and the KKT loading/unloading conditions are summarized by

$$4\rho_0 \partial_{\boldsymbol{C}\boldsymbol{C}^p} \bar{\psi} : \frac{1}{2} \dot{\boldsymbol{C}}^p = -2\dot{\beta} \partial_{\boldsymbol{C}} \Phi, \quad \Phi \leq 0, \quad \dot{\beta} \geq 0 \quad \text{and} \quad \dot{\beta}\Phi = 0, \tag{37-40}$$

where $\dot{\beta} \geq 0$ is the plastic multiplier and Φ is the yield function. Additionally, the hardening law and the hardening thermodynamical force are given, respectively, by

$$\dot{\boldsymbol{\alpha}} = -\dot{\beta} \partial_{\boldsymbol{A}} \Phi \quad \text{and} \quad \boldsymbol{A} = \rho_0 \partial_{\boldsymbol{\alpha}} \tilde{\psi}. \tag{41-42}$$

The yield criterion is determined by the KKT loading/unloading conditions (38-40).

3.3 General system of equations for the phase-field model

By replacing the previous constitutive relations into the basic governing system of equations (7) and the boundary conditions (8), enable us to rewrite the IBVP in terms of the specific free-energy potential, pseudo-potential of dissipation and the yield function.

The IBVP reads: Given the body force vector field $\boldsymbol{f}_0$, the specific density of energy a_0 and the specific heat source/sink density r_0 we want to find on $\mathcal{B}_0$, at time t, the displacement $\boldsymbol{u}$ and velocity $\boldsymbol{v}$ fields, the phase-field φ, the specific internal energy e_0 and the plastic state of the material according to

$$\begin{cases} \dot{\rho}_0 = 0, \\ \dot{\boldsymbol{u}} = \boldsymbol{v}, \\ \rho_0 \dot{\boldsymbol{v}} = \mathrm{div}_p\left(\boldsymbol{F}\boldsymbol{S}\right) + \rho_0 \boldsymbol{f}_0, \\ \partial_{\dot{\varphi}} \psi_d^n = \mathrm{div}_p\left(\rho_0 \partial_{\nabla_p \varphi}\psi\right) - \rho_0 \partial_{\varphi}\psi + \rho_0 a_0, \\ \rho_0 \dot{e_0} = \mathrm{div}_p\left(\theta \partial_{\nabla_p \theta}\psi_d^n\right) + \frac{1}{2}\boldsymbol{S} : \dot{\boldsymbol{C}} + \left(\rho_0 \partial_{\varphi}\psi + \partial_{\dot{\varphi}}\psi_d^n\right)\dot{\varphi} + \rho_0 \partial_{\nabla_p \varphi}\psi \cdot \nabla_p \dot{\varphi} + \rho_0 r_0, \\ e_0 = \psi - \theta \partial_{\theta}\psi, \\ \boldsymbol{S} = 2\rho_0 \partial_{\boldsymbol{C}}\psi + 2\partial_{\dot{\boldsymbol{C}}}\psi_d^n \quad \text{and} \quad \boldsymbol{A} = \rho_0 \partial_{\boldsymbol{\alpha}}\tilde{\psi}, \\ \Phi \leq 0, \quad \dot{\beta} \geq 0 \quad \text{and} \quad \dot{\beta}\Phi = 0, \\ 4\rho_0 \partial_{\boldsymbol{C}\boldsymbol{C}^p}\bar{\psi} : \frac{1}{2}\dot{\boldsymbol{C}}^p = -2\dot{\beta}\partial_{\boldsymbol{C}}\Phi, \\ \dot{\boldsymbol{\alpha}} = -\dot{\beta}\partial_{\boldsymbol{A}}\Phi. \end{cases} \tag{43}$$

with the boundary conditions

$$\begin{cases} \boldsymbol{u} = \boldsymbol{0} & \text{on} \quad \partial\mathcal{B}_t^{D_0} \\ \boldsymbol{u} = \bar{\boldsymbol{u}} & \text{on} \quad \partial\mathcal{B}_t^{D_u} \\ \boldsymbol{P}\boldsymbol{n}_0 = \boldsymbol{t}_0 & \text{on} \quad \partial\mathcal{B}_t^{N_\sigma} \\ \rho_0 \partial_{\nabla_p \varphi}\psi \cdot \boldsymbol{n}_0 = t_{\boldsymbol{h}0} & \text{on} \quad \partial\mathcal{B}_t^{N_h} \end{cases} \tag{44}$$

and appropriate initial conditions in $\mathcal{B}_0$ at $t = 0$ for ρ, $\boldsymbol{v}$, $\dot{\boldsymbol{v}}$, φ, θ, $\boldsymbol{C}^p$ and $\boldsymbol{\alpha}$. Herein, $\boldsymbol{u} = \boldsymbol{0}$ and $\boldsymbol{u} = \bar{\boldsymbol{u}} \neq \boldsymbol{0}$ denotes the prescribed displacements on the Dirichlet boundaries, as well as t_0 and $t_{\boldsymbol{h}0}$ denotes the macro and micro-traction prescribed on the Neumann boundaries.

The energy equation (43)(v) can be rewritten in terms of the temperature using (43)(vi). In this case, after some manipulations, we obtain

$$\begin{aligned} \rho_0 \theta \partial_{\theta\theta}\psi \dot{\theta} \quad = \quad & -\mathrm{div}_p\left(\theta \partial_{\nabla_p \theta}\psi_d^n\right) - \left(\rho_0 \theta \partial_{\theta\varphi}\psi + \partial_{\dot{\varphi}}\psi_d^n\right)\dot{\varphi} - \rho_0 \theta \partial_{\theta \nabla_p \varphi}\psi \cdot \nabla_p \dot{\varphi} - \frac{1}{2}\boldsymbol{S} : \dot{\boldsymbol{C}} - \rho_0 r_0 \\ & + \rho_0\left(\partial_{\boldsymbol{C}}\psi - \theta \partial_{\theta \boldsymbol{C}}\psi\right) : \dot{\boldsymbol{C}} + \rho_0\left(\partial_{\boldsymbol{C}^p}\psi - \theta \partial_{\theta \boldsymbol{C}^p}\psi\right) : \dot{\boldsymbol{C}}^p + \rho_0\left(\partial_{\boldsymbol{\alpha}}\psi - \theta \partial_{\theta\boldsymbol{\alpha}}\psi\right) \cdot \dot{\boldsymbol{\alpha}}. \end{aligned} \tag{45}$$

This expression is left in terms of $\dot{\varphi}$, $\dot{\boldsymbol{C}}$, $\dot{\boldsymbol{C}}^p$ and $\dot{\boldsymbol{\alpha}}$, which can be obtained of its respective expressions in (43).

4 Specialized model

In this Section we intend to specialize the proposed model for a specific free-energy potential. This potential will lead to a particular set of equations and, naturally, it can be modified for a better physical description.

4.1 Suitability of notation, thermal and plastic additional hypotheses

In order to present the following arguments related to the plasticity we need to adequate the notation and describe new hypotheses associated to the model.

We define the volume-preserving part of the gradient of deformation tensor by $\bar{\boldsymbol{F}} = J^{-\frac{1}{3}}\boldsymbol{F}$. This enable us to define alternative strain measures, for instance, the volume-preserving part of the right (total) Cauchy-Green strain tensor $\bar{\boldsymbol{C}} = \bar{\boldsymbol{F}}^T\bar{\boldsymbol{F}}$ and the left elastic Cauchy-Green strain tensor $\bar{\boldsymbol{B}}^e = \bar{\boldsymbol{F}}^e\bar{\boldsymbol{F}}^{eT}$. As in Wriggers [21, p.367], we

consider a purely volumetric thermal deformation, that is, $\boldsymbol{F}^{\theta} = J_{\theta}^{\frac{1}{3}}\boldsymbol{I}$, with J_θ given acoording [26, 27] as

$$J_\theta = \exp\left\{3\alpha_t\left(\theta - \theta_0\right)\right\}, \tag{46}$$

where α_t represents the linear thermal expansion coefficient. Moreover, it is adopted the assumption of an isochoric plastic flow, satisfied by requiring $J_p := \det(\boldsymbol{F}^p) = 1$.

From the multiplicative decomposition of $\boldsymbol{F}$ and the previous considerations we have

$$\boldsymbol{F} = J_\theta^{\frac{1}{3}}\boldsymbol{F}^e\boldsymbol{F}^p \quad \Rightarrow \quad J_e = JJ_\theta^{-1}. \tag{47}$$

4.2 Free-energy potential

The free-energy potential used in this specialization is based on [1, 6, 7, 11, 24, 28]. It is given by the sum of the elastic energy density ψ_e, the plastic energy density ψ_p, the energy density related to damage and fatigue ψ_φ and the caloric energy density ψ_θ as

$$\rho_0\psi = \psi_e\left(\boldsymbol{C}, \boldsymbol{C}^p, \Gamma_\varphi\right) + \psi_p\left(\alpha, \Gamma_\varphi\right) + \psi_\varphi\left(\varphi, \nabla_p\varphi, \mathcal{F}\right) + \psi_\theta\left(\theta\right) \quad \text{with} \quad \Gamma_\varphi = \{\varphi, \alpha\}. \tag{48}$$

Following [11, 24, 28], the elastic energy density ψ_e of the material subject to damage is given according to

$$\psi_e\left(\boldsymbol{C}, \boldsymbol{C}^p, \Gamma_\varphi\right) = g_e^{(1)}\left(\Gamma_\varphi\right)\mathcal{E}_0^+\left(J_e, \bar{\boldsymbol{C}}, \boldsymbol{C}^p\right) + g_e^{(2)}\left(\Gamma_\varphi\right)\mathcal{E}_0^-\left(J_e\right), \tag{49}$$

with the positive and negative virgin elastic energy densities given, respectively, by

$$\mathcal{E}_0^+\left(J_e, \bar{\boldsymbol{C}}, \boldsymbol{C}^p\right) = \begin{cases} U\left(J_e\right) + \bar{W}\left(\bar{\boldsymbol{C}}, \boldsymbol{C}^p\right), & J_e \geq 1 \\ \bar{W}\left(\bar{\boldsymbol{C}}, \boldsymbol{C}^p\right), & J_e < 1 \end{cases} \quad \text{and} \quad \mathcal{E}_0^-\left(J_e\right) = \begin{cases} 0, & J_e \geq 1 \\ U\left(J_e\right), & J_e < 1 \end{cases}, \tag{50-51}$$

where

$$U\left(J_e\right) = \frac{K}{2}\left[\frac{1}{2}\left(J_e^2 - 1\right) - \ln\left(J_e\right)\right] \quad \text{and} \quad \bar{W}\left(\bar{\boldsymbol{C}}, \boldsymbol{C}^p\right) = \frac{G}{2}\left(\bar{\boldsymbol{C}} : \boldsymbol{C}^{p-1} - 3\right). \tag{52-53}$$

Herein, K and G represents the bulk and shear module, respectively.

The plastic energy density of a damaged material is given by

$$\psi_p\left(\alpha, \Gamma_\varphi\right) = g_p\left(\Gamma_\varphi\right)\mathcal{H}_0\left(\alpha\right), \tag{54}$$

where $\boldsymbol{\alpha}$ has just one component α, namely, the accumulated plastic strain and the plastic energy density $\mathcal{H}_0$ is assumed to correspond to the Voce hardening law [29] given in terms of the yield stress σ_y and material parameters r_p and s_p, as

$$\mathcal{H}_0\left(\alpha\right) = \sigma_y\alpha + r_p\left[\alpha + \frac{1}{s_p}\exp\left(-s_p\alpha\right)\right]. \tag{55}$$

From [1, 7], the energy density of damage and fatigue processes is described by

$$\psi_\varphi\left(\varphi, \nabla_p\varphi, \mathcal{F}\right) = G_c\left(\frac{\gamma}{2}\left|\boldsymbol{F}^{-t}\nabla_p\varphi\right|^2 + \frac{1}{\gamma}\mathcal{H}\left(\varphi\right)\right) + \frac{1}{\gamma}\mathcal{F}\mathcal{H}_f\left(\varphi\right), \tag{56}$$

where the non-usual term $\boldsymbol{F}^{-T}\nabla_p\varphi$ refers to the pull-back (to the Lagrangian configuration) of the spatial gradient $\nabla_x\varphi$. As described in [7], this consideration generate additional terms that differs of other phase-field models already developed.

Lastly, the purely caloric energy density is

$$\psi_\theta\left(\theta\right) = -c_V\theta\ln\left(\theta\right), \tag{57}$$

where ln denotes the natural logarithm and $c_V > 0$ is the volumetric heat capacity of the material.

From (43)(viii) and the free-energy density (48), the second Piola-Kirchhoff stress tensor can be expressed by the sum of the following terms

$$\boldsymbol{S} = \boldsymbol{S}_c + \boldsymbol{S}_\varphi + \boldsymbol{S}_d, \tag{58}$$

where the "conventional" second Piola-Kirchhoff stress tensor is given from (49) as

$$\boldsymbol{S}_c = 2\partial_{\boldsymbol{C}}\psi_e = g_e^{(1)}\left(\Gamma_\varphi\right)\boldsymbol{S}_c^{+} + g_e^{(2)}\left(\Gamma_\varphi\right)\boldsymbol{S}_c^{-}, \tag{59}$$

with the terms $\boldsymbol{S}_c^{\pm}$ given by

$$\begin{aligned}
\boldsymbol{S}_c^{+} &= \begin{cases} J_e U'\left(J_e\right)\boldsymbol{C}^{-1} + GJ_e^{-\frac{2}{3}}\left[\boldsymbol{C}^{p-1} - \dfrac{1}{3}\left(\boldsymbol{C}:\boldsymbol{C}^{p-1}\right)\boldsymbol{C}^{-1}\right], & J_e \geq 1 \\ GJ_e^{-\frac{2}{3}}\left[\boldsymbol{C}^{p-1} - \dfrac{1}{3}\left(\boldsymbol{C}:\boldsymbol{C}^{p-1}\right)\boldsymbol{C}^{-1}\right], & J_e < 1 \end{cases}, \\
\boldsymbol{S}_c^{-} &= \begin{cases} \boldsymbol{0}, & J_e \geq 1 \\ J_e U'\left(J_e\right)\boldsymbol{C}^{-1}, & J_e < 1 \end{cases},
\end{aligned} \tag{60}$$

and the remaining terms by

$$\boldsymbol{S}_\varphi = 2\partial_{\boldsymbol{C}}\psi_\varphi = -G_c\gamma\left(\boldsymbol{C}^{-1}\nabla_p\varphi\right)\otimes\left(\boldsymbol{C}^{-1}\nabla_p\varphi\right) \quad \text{and} \quad \boldsymbol{S}_d = 2\partial_{\dot{\boldsymbol{C}}}\psi_d^n = 2\tilde{b}_d\dot{\boldsymbol{C}}. \tag{61-62}$$

The Kirschhoff stress tensor $\boldsymbol{\tau}_c$, related to the conventional part of the stress tensor, can be computed by the push-forward of $\boldsymbol{S}_c$, that is, $\boldsymbol{F}\boldsymbol{S}_c\boldsymbol{F}^T = \boldsymbol{\tau}_c$. This measure appear in the return mapping scheme presented by Borden *et al.* [6], that fill the gap concerning isochoric plastic flow formulations.

4.3 Non-plastic pseudo-potential of dissipation

We assume the non-plastic pseudo-potential of dissipation for the degraded materials similarly in [7] by

$$\psi_d^n = \frac{1}{2}\tilde{\lambda}\left(\tilde{\Gamma}\right)\left|\dot{\varphi}\right|^2 + \frac{1}{2}\tilde{b}_d\left(\tilde{\Gamma}\right)\left|\dot{\boldsymbol{C}}\right|^2 + \frac{1}{2}g_\theta\left(\Gamma_\varphi\right)\tilde{c}_\theta\left(\tilde{\Gamma}\right)\left|\nabla_p\theta\right|^2, \tag{63}$$

where $\tilde{\Gamma}$ is the set of variables defined in (24), and the nonnegative coefficients $\tilde{\lambda}$, $\tilde{b}_d$ and $\tilde{c}_\theta$ are dependent on the material (see details in [7]). In particular, we consider $\tilde{\lambda} := (1-\varphi)/\tilde{c}$, where $\tilde{c}$ is an additional parameter and represents the damage rate.

4.4 Elasto-plastic rules

Let us consider that the yielding is determined by the Mises-Huber yield condition. Given in terms of the conventional Kirchhoff stress tensor $\boldsymbol{\tau}_c$, the yield function is defined by

$$\Phi = \bar{\Phi}\left(\boldsymbol{\tau}_c, \boldsymbol{A}\right) = \left\|\mathrm{dev}(\boldsymbol{\tau}_c)\right\| - \sqrt{\frac{2}{3}}\boldsymbol{A}. \tag{64}$$

For the sake of simplicity, Φ is assumed independent of $\tilde{\Gamma}$.

From the governing equations given in (43), the free-energy introduced in (48) and the yield function given in (64), the hardening thermodynamical force and hardening law are given, respectively, by

$$\boldsymbol{A} = \rho_0\,\partial_\alpha\psi = \partial_\alpha g_e^{(1)}\mathcal{E}_0^{+} + \partial_\alpha g_e^{(2)}\mathcal{E}_0^{-} + g_p\partial_\alpha\mathcal{H}_0 + \partial_\alpha g_p\mathcal{H}_0 \quad \text{and} \quad \dot{\boldsymbol{\alpha}} = -\dot{\beta}\partial_{\boldsymbol{A}}\Phi = \sqrt{\frac{2}{3}}\dot{\beta}. \tag{65-66}$$

The plastic flow rule in the Lagrangian configuration is given, by replacing (48) into (37), by

$$\mathrm{DEV}\left(\dot{\boldsymbol{C}}^{p-1}\right) = -\frac{2}{3}J_\theta^{\frac{2}{3}}\dot{\beta}\boldsymbol{C}:\boldsymbol{C}^{p-1}\boldsymbol{N} \quad \text{where} \quad \boldsymbol{N} = \boldsymbol{F}^{-1}\boldsymbol{n}\boldsymbol{F}^{-t} \quad \text{and} \quad \boldsymbol{n} = \frac{\mathrm{dev}(\boldsymbol{\tau}_c)}{\left\|\mathrm{dev}(\boldsymbol{\tau}_c)\right\|}. \tag{67-69}$$

5 Frictionless contact problem description

Let us assume two distinct bodied that at time $t = 0$ occupies the configurations $\mathcal{B}_0^\gamma \subset \mathbb{R}^3$ with Lagrangian coordinates $\boldsymbol{p}^\gamma$ for $\gamma = 1, 2$. Moreover, let us consider ϕ^γ their respective mappings to the current configuration, as illustrated in Figure 1.

Physically, the contact problem is characterized by the interaction between different parts of bodies during the mechanical deformation process, where interaction forces between the contact parts arise to prevent the penetration not physically admissible. Mathematically, this means that, at any time t, we must ensure $\mathcal{B}_t^1 \cap \mathcal{B}_t^2 = \emptyset$.

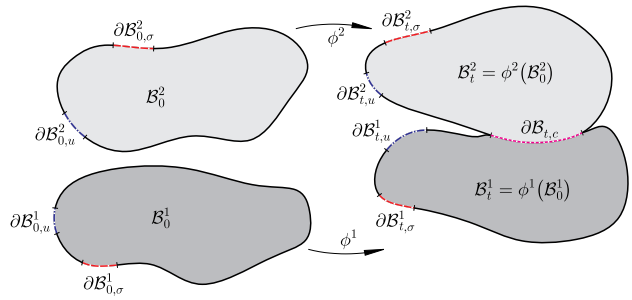

Figure 1. Kinematics of the finite deformation contact problem.

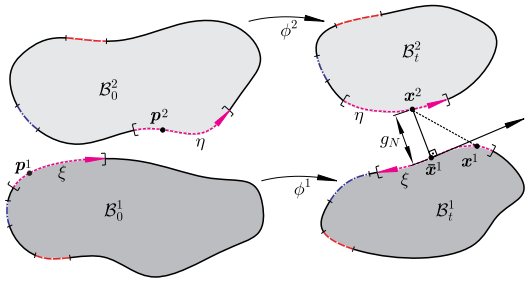

Figure 2. Current configuration of the bodies.

In order to develop the main ideas related to the frictionless contact, we assume the boundary $\partial\mathcal{B}_t^\gamma$ of $\mathcal{B}^\gamma$ consisting of three parts, namely, $\partial\mathcal{B}_{t,\sigma}^\gamma$, $\partial\mathcal{B}_{t,u}^\gamma$ and $\partial\mathcal{B}_{t,c}^\gamma$ subject, respectively, to the action of stresses, displacements and the so-called contact surface, where the bodies $\mathcal{B}_t^1$ and $\mathcal{B}_t^2$ are, possibly, in contact. These boundaries must be such that $\partial\mathcal{B}_{t,\sigma}^\gamma \cup \partial\mathcal{B}_{t,u}^\gamma \cup \partial\mathcal{B}_{t,c}^\gamma = \partial\mathcal{B}_t^\gamma$ and $\partial\mathcal{B}_{t,\sigma}^\gamma \cap \partial\mathcal{B}_{t,u}^\gamma \cap \partial\mathcal{B}_{t,c}^\gamma = \emptyset$. Once contact occurs, an impenetrability condition must be verified. A generic pair of contacting points $\boldsymbol{p}^\gamma \in \partial\mathcal{B}_{0,c}^\gamma$ and its current positions $\boldsymbol{x}^\gamma = \phi^\gamma(\boldsymbol{p}^\gamma, t) \in \partial\mathcal{B}_{t,c}^\gamma$ must be considered in order to express such condition. In addition, let us consider $\xi, \eta \in [-1, 1]$ local coordinates on the contact boundaries. Such considerations were illustrated in Figure 2.

The solution of a frictionless contact problem can be obtained from the minimization of the total potential energy subject to m inequality constraints $g_i(\boldsymbol{u})$ of non-penetration between bodies. Mathematically, we can define the problem as

$$(P) \begin{cases} min & \Psi_{tot}(\boldsymbol{u}) = \Psi_s(\boldsymbol{u}) + \Psi_c(\boldsymbol{u}, \phi^\gamma) \\ s.t. & g_N(\boldsymbol{u}) \geq 0 \end{cases}, \tag{70}$$

where Ψ_{tot} is the total potential energy, Ψ_s is the potential energy of the mechanical system obtained from the free-energy potential (Eq. (48)) and Ψ_c is the potential energy of the contact contribution. The constraints are given by the normal gap function g_N (Fig. 2), that represents the specific non-penetration condition of bodies. The normal gap function can be defined in terms of the normal vector $\nu\left(\bar{\xi}\right)$ at a specific target point $\bar{\boldsymbol{x}}^1\left(\bar{\xi}\right)$ as

$$g_N(\boldsymbol{u}) = \left[\boldsymbol{x}^2 - \bar{\boldsymbol{x}}^1\left(\bar{\xi}\right)\right] \cdot \nu\left(\bar{\xi}\right). \tag{71}$$

For $g_N = 0$, a perfect contact occurs. In a penetration condition between bodies, $g_N > 0$, and for a non-penetration condition, $g_N < 0$.

We can write the variation of the total potential energy for the contact problem using the Principle of Virtual Work (PVW) as

$$\delta\Psi_{tot}\left(\boldsymbol{u}\right) = \delta\Psi_s\left(\boldsymbol{u}\right) + \delta\Psi_c\left(\boldsymbol{u}\right), \tag{72}$$

where $\delta\Psi_s$ is the description of the system virtual work. Further detailed description on the derivation of the weak form of the BVP, including hypereslasticity behavior, can be found in [30, 31]. The contact virtual work $\delta\Pi_c$ is defined as

$$\delta\Psi_c\left(\boldsymbol{u}\right) = \int_{\Gamma_c} \boldsymbol{t} \cdot \delta\boldsymbol{g} d\Gamma_c, \tag{73}$$

where $\boldsymbol{t}$ is the contact traction vector field [32] and $\delta\boldsymbol{g}$ the variation of the gap vector. We can rewrite the virtual work associated to the contact contribution using the Augmented Lagrangian method as

$$\delta\Psi^{AL} = \int_{\Gamma_c} t_N \delta g_N dA, \tag{74}$$

where t_N is the normal contact stress and δg_N is the variation of the normal gap, which are defined as

$$t_N := \langle \lambda_N + \epsilon_N g_N \rangle \quad \text{and} \quad \delta g_N := \delta\left[\left(\boldsymbol{x}^2 - \bar{\boldsymbol{x}}^1\left(\bar{\xi}\right)\right) \cdot \nu\left(\bar{\xi}\right)\right]. \tag{75-76}$$

The scalars λ_N and ϵ_N are, respectively, the normal Lagrange multiplier and the penalty parameter. The coordinate $\boldsymbol{\xi} = (\bar{\xi})$ denotes the parameterization of the boundary surface Γ_c by convective coordinates widely

used in the literature for solving contact problems [31–34]. In the present work, we use the Uzawa algorithm [35] to solve the resulting system of equations.

The resultant problem becomes subject to the following KKT constraint equations:

$$\lambda_N \geq 0, \quad g_N \leq 0 \quad \text{and} \quad \lambda_N g_N = 0. \tag{77-79}$$

Further details of the contact element used in this work, contact solvers and complete overviews about contact mechanics can be found in [31, 36–38].

6 Numerical approximation

The semi-implicit/explicit time integration scheme presented in Haveroth *et al.* [7] is conveniently modified to solve the motion and damage equations, in this order. For the sake of convenience, in this study we disregard the temperature effects maintaning a fixed temperature of $\theta = 298.15$ K. In each time step, the resulting linearized system of equations are solved, using the conjugate gradient method with the diagonal (CGD) pre-conditioner. The upgraded Lagrangian formulation is employed to perform the numerical integrations, as a manner to deal more easily the proposed finite strain formulation.

In subsequent sections we describe the discretization of the motion and damage equations by using the finite element method and the most appropriate time integration procedure. In order to present them, let us consider the time interval solution $[0, T]$ in discrete time steps t_n with a time step increment $\Delta t = t_{n+1} - t_n$ for $n = 0, 1, 2, \ldots$. The variables $(\cdot)$ evaluated at time t_{n+1} are denoted by $(\cdot)_{n+1}$. Moreover, the superscript $(\cdot)^i$ means that $(\cdot)$ is evaluated at the i-th iteration of the Newton-Raphson (NR) procedure.

Moreover, we consider a finite element mesh such that

$$\mathcal{B}_{n+1} = \mathop{\mathrm{A}}_{k=1}^{nel} \mathcal{B}_{n+1}^k, \tag{81}$$

where $\mathcal{B}_{n+1}^k$ is the domain of the k-th element, or k_c-th contact element, at time t_{n+1}, nel is the number of elements and A represents the assembling procedure. For each k-th element, the approximations of the fields are written as a linear combination of η local nodal basis function N_j as

$$\boldsymbol{u}^k = \boldsymbol{N}\hat{\boldsymbol{u}}^k, \quad \boldsymbol{v}^k = \boldsymbol{N}\hat{\boldsymbol{v}}^k, \quad \dot{\boldsymbol{v}}^k = \boldsymbol{N}\dot{\hat{\boldsymbol{v}}}^k, \quad \boldsymbol{f}^k = \boldsymbol{N}\hat{\boldsymbol{f}}^k, \quad \varphi^k = \bar{\boldsymbol{N}}\hat{\varphi}^k, \quad \mathcal{F}^k = \bar{\boldsymbol{N}}\hat{\mathcal{F}}^k \quad \text{and} \quad \theta^k = \bar{\boldsymbol{N}}\hat{\theta}^k, \tag{82-88}$$

where the symbol $\hat{(\cdot)}$ represents the nodal values of the field $(\cdot)$ and the matrices $\bar{\boldsymbol{N}}$ and $\boldsymbol{N}$ are respectively defined by

$$\bar{\boldsymbol{N}} = \begin{bmatrix} N_1 & N_2 & \cdots & N_\eta \end{bmatrix} \quad \text{and} \quad \boldsymbol{N} = \begin{bmatrix} N_1 & 0 & N_2 & 0 & \cdots & N_\eta & 0 \\ 0 & N_1 & 0 & N_2 & 0 & \cdots & N_\eta \end{bmatrix}. \tag{89-90}$$

The interpolation of the displacement, velocity, damage and temperature gradients are given in terms of linear combinations of the shape function global derivatives by

$$\boldsymbol{E}^k = \boldsymbol{B}\hat{\boldsymbol{u}}^k, \quad \boldsymbol{D}^k = \boldsymbol{B}\hat{\boldsymbol{v}}^k, \quad \nabla\varphi^k = \bar{\boldsymbol{B}}\hat{\varphi}^k \quad \text{and} \quad \nabla\theta^k = \bar{\boldsymbol{B}}\hat{\theta}^k, \tag{91-94}$$

where $\bar{\boldsymbol{B}}$ and $\boldsymbol{B}$ are given respectively by

$$\bar{\boldsymbol{B}} = \begin{bmatrix} N_{1,x} & N_{2,x} & \cdots & N_{\eta,x} \\ N_{1,y} & N_{2,y} & \cdots & N_{\eta,y} \end{bmatrix} \quad \text{and} \quad \boldsymbol{B} = \begin{bmatrix} N_{1,x} & 0 & N_{2,x} & 0 & \cdots & N_{\eta,x} & 0 \\ N_{1,y} & 0 & N_{2,y} & 0 & \cdots & N_{\eta,y} & 0 \\ 0 & N_{1,x} & 0 & N_{2,y} & \cdots & 0 & N_{\eta,x} \\ 0 & N_{1,y} & 0 & N_{2,x} & \cdots & 0 & N_{\eta,y} \end{bmatrix}. \tag{95-96}$$

The global form of the operators in next sections are indicated without the subscript k, obtained by applying the assembling procedure for all element contributions.

6.1 Motion equation

The linearization of the motion equation (43)(ii-iii) for a quasi-static situation is already performed in [39, p.496]. Here, we modify it by assuming the updated Lagrangian configuration and a dynamic situation, solved by adopting

the Newmark method for time discretization [7]. The velocity and acceleration vectors are approximated using the updated values of the displacement vector $\boldsymbol{u}_{n+1}$ as

$$\boldsymbol{v}_{n+1} = \chi_4 \left(\boldsymbol{u}_{n+1} - \boldsymbol{u}_n\right) + \chi_5 \boldsymbol{v}_n + \chi_6 \dot{\boldsymbol{v}}_n \quad \text{and} \quad \dot{\boldsymbol{v}}_{n+1} = \chi_1 \left(\boldsymbol{u}_{n+1} - \boldsymbol{u}_n\right) - \chi_2 \boldsymbol{v}_n - \chi_3 \dot{\boldsymbol{v}}_n, \tag{97-98}$$

where $\chi_1, \ldots, \chi_6$ are given in terms of the Newmark coefficients $\tilde{\gamma}$ and $\tilde{\beta}$ (here $\tilde{\gamma} = 0.5$ and $\tilde{\beta} = 0.25$) by

$$\chi_1 = \frac{1}{\tilde{\beta}\Delta t^2}, \quad \chi_2 = \frac{1}{\tilde{\beta}\Delta t}, \quad \chi_3 = \frac{1-2\tilde{\beta}}{2\tilde{\beta}}, \quad \chi_4 = \frac{\tilde{\gamma}}{\tilde{\beta}\Delta t}, \quad \chi_5 = 1 - \frac{\tilde{\gamma}}{\tilde{\beta}} \quad \text{and} \quad \chi_6 = \left(1 - \frac{\tilde{\gamma}}{2\tilde{\beta}}\right)\Delta t. \tag{99-104}$$

As result, we obtain the residue and jacobian for the k-th element given by

$$\begin{aligned} \boldsymbol{r}_m^k = &\int_{\mathcal{B}_n^k} \rho_0 \boldsymbol{N}^T \boldsymbol{N} \; dV_n^k \left[\chi_1 \left(\hat{\boldsymbol{u}}_{n+1}^k - \hat{\boldsymbol{u}}_n^k\right) - \chi_2 \hat{\boldsymbol{v}}_n^k - \chi_3 \dot{\hat{\boldsymbol{v}}}_n^k\right] + \int_{\mathcal{B}_n^k} \boldsymbol{B}^t \tilde{\boldsymbol{F}}_\Delta^t \left\{\boldsymbol{S}_{n+1}^k\right\} \; dV_n^k \\ &- \int_{\mathcal{B}_n^k} \rho_0 \boldsymbol{N}^T \boldsymbol{N} \; dV_n^k \hat{\boldsymbol{f}}_{n+1}^k + \int_{\partial\mathcal{B}_{n,c}^k} t_N \delta g_N \; d\Gamma_{c_n}^{k_c}, \end{aligned} \tag{105}$$

$$\begin{aligned} \boldsymbol{J}_m^k = &\chi_1 \int_{\mathcal{B}_n^k} \rho_0 \boldsymbol{N}^T \boldsymbol{N} \; dV_n^k + \int_{\mathcal{B}_n^k} \left[\boldsymbol{B}^t \tilde{\boldsymbol{S}}_{n+1}^k \boldsymbol{B} + \boldsymbol{B}^t \tilde{\boldsymbol{F}}_\Delta^t \boldsymbol{D}_{n+1}^{\text{ep}} \tilde{\boldsymbol{F}}_\Delta \boldsymbol{B}\right] \; dV_n^k \\ &+ \int_{\partial\mathcal{B}_{n,c}^k} \left[\Delta t_N \delta g_N + t_N \Delta \delta g_N\right] \; d\Gamma_{c_n}^{k_c}, \end{aligned} \tag{106}$$

with their global versions evaluated by applying the assemble operator over the element contributions. Herein, the symbol $\{(\cdot)\}$ in the above terms means that the tensor $(\cdot)$ is represented using Voigt notation, that is,

$$\left\{\boldsymbol{S}_{n+1}^k\right\} = \begin{bmatrix} S_{11,n+1}^k & S_{22,n+1}^k & S_{12,n+1}^k \end{bmatrix}^t. \tag{107}$$

Moreover, the second order tensors $\tilde{\boldsymbol{S}}_{n+1}^k$ and $\tilde{\boldsymbol{F}}_\Delta$, described by

$$\tilde{\boldsymbol{S}}_{n+1}^k = \begin{bmatrix} S_{11,n+1}^k & S_{12,n+1}^k & 0 & 0 \\ S_{12,n+1}^k & S_{22,n+1}^k & 0 & 0 \\ 0 & 0 & S_{11,n+1}^k & S_{12,n+1}^k \\ 0 & 0 & S_{12,n+1}^k & S_{22,n+1}^k \end{bmatrix} \quad \text{and} \quad \tilde{\boldsymbol{F}}_\Delta = \begin{bmatrix} F_{\Delta,11} & 0 & F_{\Delta,21} & 0 \\ 0 & F_{\Delta,12} & 0 & F_{\Delta,22} \\ F_{\Delta,12} & F_{\Delta,11} & F_{\Delta,22} & F_{\Delta,21} \end{bmatrix},$$

are given in terms of the second Piola-Kirschhoff stress tensor $\boldsymbol{S}_{n+1}^k$ and the increment of gradient of deformation $\boldsymbol{F}_\Delta := \boldsymbol{F}_{n+1}(\boldsymbol{F}_n)^{-1}$. Lastly, the tensor $\boldsymbol{D}_{n+1}^{\text{ep}}$ refers to the consistent elasto-plastic tangent modulus evaluated numerically by using complex derivative as presented in Haveroth [25]. Further details of the integrals on contact surfaces $\Gamma_{c_n}^{k_c}$ can be found in [31, 38].

It is important to highlight that the second Piola-Kirchhoff stress tensor $\boldsymbol{S}_{n+1}^k$ must be evaluated at configuration $\mathcal{B}_n^k$. From (58), this tensor is given by the sum

$$\boldsymbol{S}_{n+1}^k = \boldsymbol{S}_{c,n+1}^k + \boldsymbol{S}_{\varphi,n+1}^k + \boldsymbol{S}_{d,n+1}^k. \tag{108}$$

The conventional stress term $\boldsymbol{S}_{c,n+1}^k$ is obtained by using the return mapping algorithm. From (61-62), freezing the damage terms due to the adopted semi-implicit strategy and from the push-forward of the gradient term $\nabla_p(\cdot) = \boldsymbol{F}_n^t \nabla_{x_n}(\cdot)$, we have

$$\boldsymbol{S}_{\varphi,n+1}^k = -G_c \gamma \left(\boldsymbol{C}_{n+1}^{-1} \boldsymbol{F}_n^t \nabla_{x_n} \varphi_n\right) \otimes \left(\boldsymbol{C}_{n+1}^{-1} \boldsymbol{F}_n^t \nabla_{x_n} \varphi_n\right). \tag{109}$$

The remaining term is computed by using a simple finite difference as

$$\boldsymbol{S}_{d,n+1}^k = 2\tilde{b}_d \frac{\boldsymbol{C}_{n+1} - \boldsymbol{C}_n}{\Delta t}. \tag{110}$$

Once computed $\boldsymbol{u}_{n+1}$, the acceleration and velocity fields are updated by using the relations (98-97).

6.2 Damage equation

The trapezoidal time integration rule with appropriate modifications are applied for the damage equation, obtained by replacing (48) and (63) into (43)(iv). These adjustments contemplate the semi-implicit strategy with the fatigue variable freezed at past time step and additional numeric considerations (see details in [7]).

By using the finite element approximations and the push-forward of the gradient term $\nabla_p(\cdot) = \boldsymbol{F}_n^t \nabla_{x_n}(\cdot)$, we obtain the descritized residue and jacobian for the k-th element as

$$\begin{aligned} \boldsymbol{r}_d^k &= \int_{\mathcal{B}_n^k} \Psi_d^k \bar{\boldsymbol{N}}^T \, dV_n^k + \int_{\mathcal{B}_n^k} \frac{\Delta t \gamma G_c}{2\tilde{\lambda}_n} \bar{\boldsymbol{B}}^t \boldsymbol{F}_n \left(\boldsymbol{C}_{n+1}^{-1} \boldsymbol{F}_n^t \bar{\boldsymbol{B}} \hat{\varphi}_{n+1}^k + \boldsymbol{C}_n^{-1} \boldsymbol{F}_n^t \bar{\boldsymbol{B}} \hat{\varphi}_n^k \right) dV_n^k, \\ \boldsymbol{J}_d^k &= \int_{\mathcal{B}_n^k} d\Psi_d^k \bar{\boldsymbol{N}}^T \bar{\boldsymbol{N}} \, dV_n^k + \int_{\mathcal{B}_n^k} \frac{\Delta t \gamma G_c}{2\tilde{\lambda}_n} \bar{\boldsymbol{B}}^t \boldsymbol{F}_n \boldsymbol{C}_{n+1}^{-1} \boldsymbol{F}_n^t \bar{\boldsymbol{B}} \, dV_n^k, \end{aligned} \tag{111}$$

where

$$\begin{aligned} \Psi_d^k &= \bar{\boldsymbol{N}} \left(\hat{\varphi}_{n+1} - \hat{\varphi}_n \right) + \frac{\Delta t \gamma g_c}{2 d\tilde{\lambda}_n} \left(\bar{\boldsymbol{B}} \hat{\varphi}_n \right)^t \left(\boldsymbol{F}_n \boldsymbol{C}_{n+1}^{-1} \boldsymbol{F}_n^t + \boldsymbol{F}_n \boldsymbol{C}_n^{-1} \boldsymbol{F}_n^t \right) \bar{\boldsymbol{B}} \hat{\varphi}_n \\ &\quad + \frac{\Delta t}{2\tilde{\lambda}_n} \Big(\partial_\varphi g_{e,n+1}^{(1)} \mathcal{E}_{0,n+1}^+ + \partial_\varphi g_{e,n+1}^{(2)} \mathcal{E}_{0,n+1}^- + \partial_\varphi g_{p,n+1} H_{0,n+1} + \partial_\varphi g_{e,n}^{(1)} \mathcal{E}_{0,n}^+ \\ &\quad + \partial_\varphi g_{e,n}^{(2)} \mathcal{E}_{0,n}^- + \partial_\varphi g_{p,n} H_{0,n} \Big) + \frac{\Delta t G_c}{2\tilde{\lambda}_n \gamma} \bar{\boldsymbol{N}} \left(\hat{\varphi}_{n+1} + \hat{\varphi}_n \right), \\ d\Psi_d^k &= \left(1 + \frac{\Delta t G_c}{2\tilde{\lambda}_n \gamma} \right) + \frac{\Delta t}{2\tilde{\lambda}_n} \left(\partial_{\varphi\varphi} g_{e,n+1}^{(1)} \mathcal{E}_{0,n+1}^+ + \partial_{\varphi\varphi} g_{e,n+1}^{(2)} \mathcal{E}_{0,n+1}^- + \partial_{\varphi\varphi} g_{p,n+1} H_{0,n+1} \right), \end{aligned} \tag{112}$$

and

$$\tilde{\lambda}_n = \left(1 - \bar{\boldsymbol{N}} \hat{\varphi}_n \right) / \tilde{c} \quad \text{and} \quad d\tilde{\lambda}_n = \left(1 - \bar{\boldsymbol{N}} \hat{\varphi}_n \right)^2 / \tilde{c}. \tag{113-114}$$

7 Results

In this section, we present the results obtained for a large deformation frictionless fracture impact problem between a beam and a wedge as shown in Fig. 3. The geometry and boundary conditions are presented in Fig. 3. The beam was completely fixed at the left edge and the wedge was constrained in the x direction at the right edge. A vertical displacement $u_y = 1.0\,[UL]$ was applied on the bottom of the wedge considering a total integration time $T = 1.0\,s$ with a time step $\Delta t = 10^{-3}\,s$. The mesh is composed of linear quadrilateral elements as illustrated in Fig. 4. The convergence tolerances used for the CGD was 10^{-8} and for the Newton-Raphson procedures was 10^{-6}. The penalty parameters used on the Augmented Lagrangian method were $\epsilon_N = 1.0 \times 10^8$ and $\Delta\epsilon_N = 1.0 \times 10^8$. We adopted $P + 1$ Gauss-Legendre integration points for the contact elements that were enough to achieve satisfatory results. The tolerances for the gap function and contact stress were 10^{-2}. The remaining material and phase-field parameters used in the simulation are summarized in Table 1.

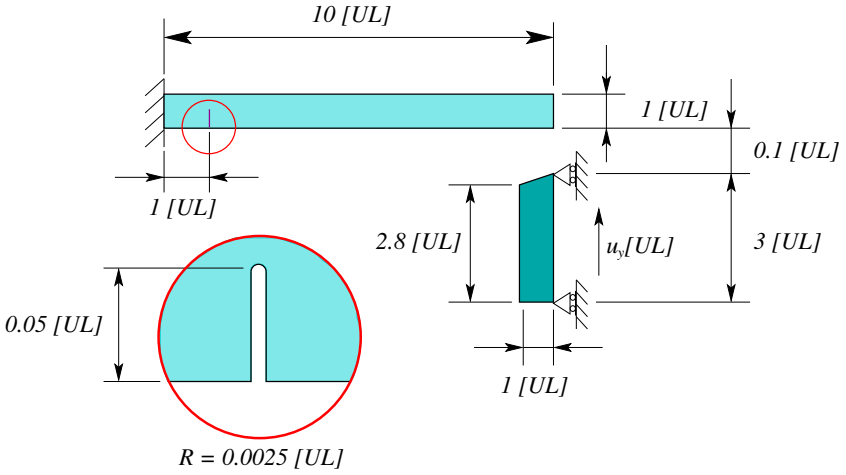

Figure 3. Impact problem representation with domain dimensions and initial conditions.

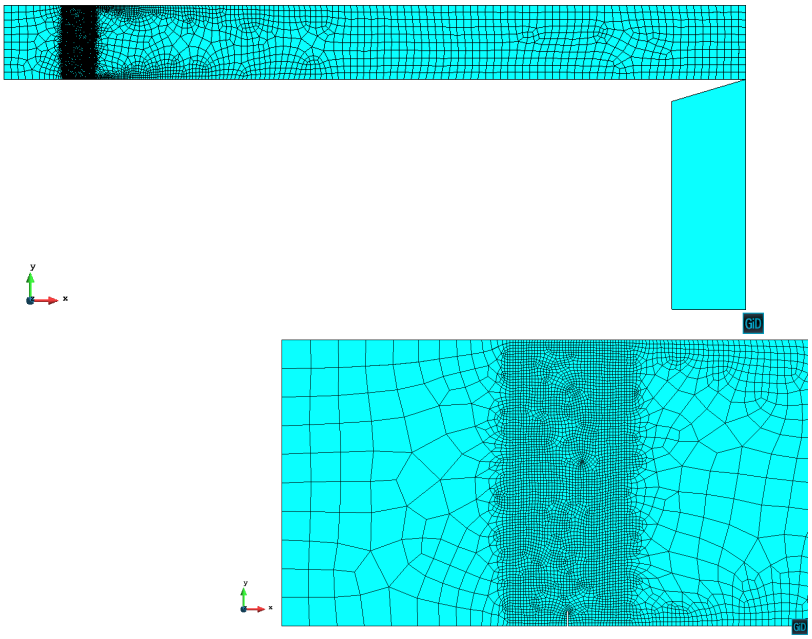

Figure 4. Mesh composed of linear quadrilateral elements.

Young modulus [GPa]	E	72.0	Yield stress [MPa]	σ_y	368.0
Poisson's ratio	ν	0.33	Plastic parameter [MPa]	r_p	78.0
Density [kg/m^3]	ρ_0	2810.0	Plastic parameter	s_p	32.0
Phase layer width [mm]	γ	0.5	Viscous dissipation [N.s/m^2]	$\tilde{b}_d$	3.0×10^6
Damage rate [m^2/N.s]	$\tilde{c}$	0.001	Phase-field parameter	ζ	1.0
Griffith fracture energy [N/m]	g_c	4950.6			

Table 1. Parameters used in the simulation.

Figure 5 shows the damage distribution for different time steps of the solution by assuming the degradation functions $g_p = 1$ and $g_e^{(1)} = g_e^{(2)} = (1-\varphi)^2$. We observe that the crack initiates close to the initial notch and propagates vertically, concerning to the x-axis, characterizing, qualitatively, a brittle fracture in an elasto-plastic material. The quality of the crack description was limited by the size of the elements in the mesh.

8 Conclusions

In this paper, we proposed a thermodynamically consistent non-isothermal phase-field model to describe the effects of damage and fracture in elasto-plastic materials under finite strain. The contact constraints were introduced conveniently in the weak form of the motion equation. We performed a frictionless impact fracture problem simulation showing crack initialization and subsequent propagation in agreement with expected results.

Acknowledgements

The authors would like to thank the São Paulo Research Foundation (FAPESP) under grants 2013/50238-3 and 2015/20188-0, the Coordination for the Improvement of Higher Education Personnel (CAPES) and also the National Council for Scientific and Technological Development (CNPq) under grant 306182/2014-9 and 308373/2016-2 for their support.

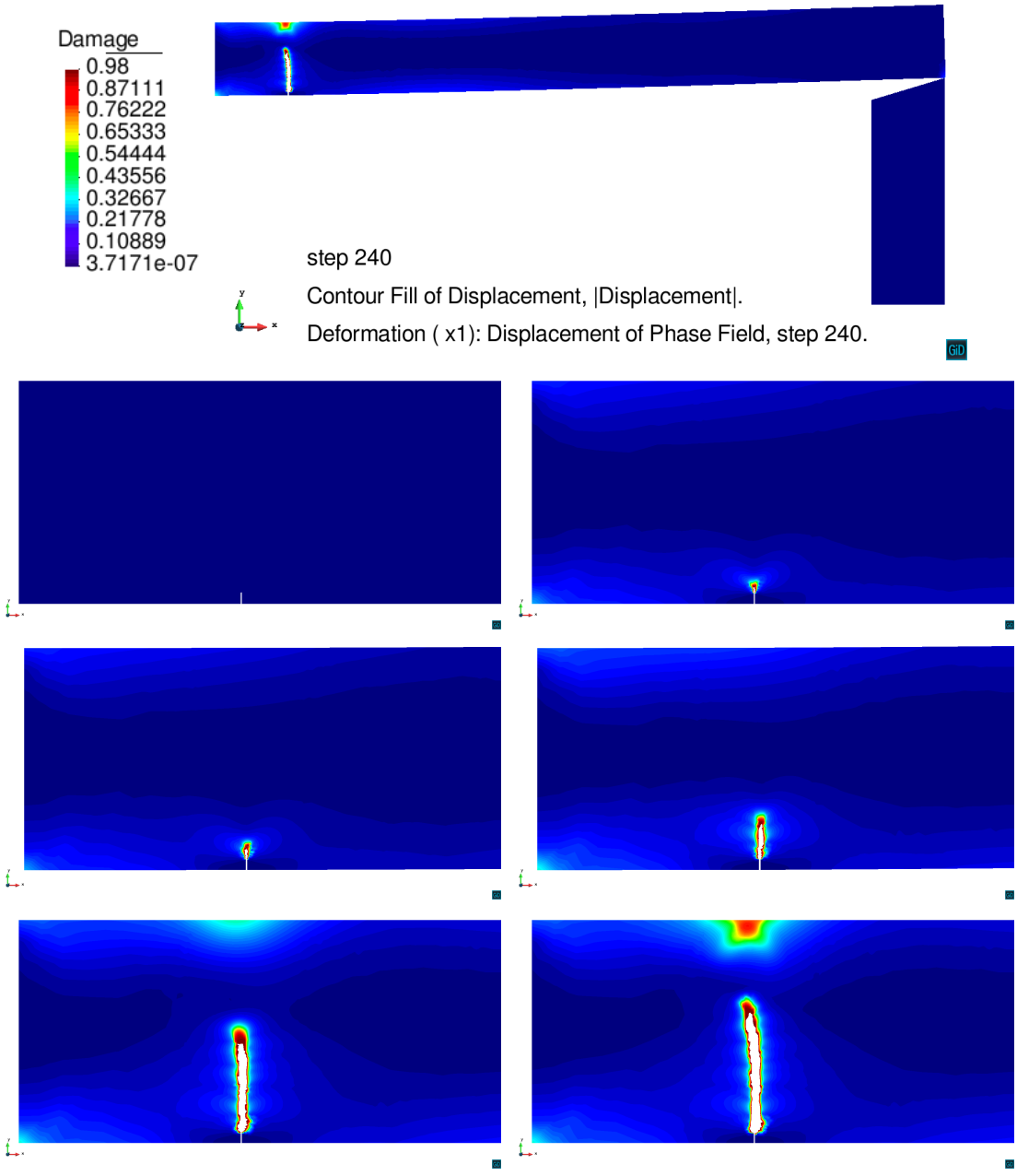

Figure 5. Damage distribution for the deformed geometry at $t = 0.240$ and details at $t = 0.001$, 0.130, 0.150, 0.180, 0.220 and 0.240 s, respectively.

References

[1] Boldrini, J. L., de Moraes, E. A. B., Chiarelli, L. R., Fumes, F. G., & Bittencourt, M. L., 2016. A non-isothermal thermodynamically consistent phase field framework for structural damage and fatigue. *Computer Methods in Applied Mechanics and Engineering*, vol. 312, pp. 395–427.
[2] Miehe, C., Hofacker, M., & Welschinger, F., 2010a. A phase field model for rate-independent crack propagation: robust algorithmic implementation based on operator splits. *Computer Methods in Applied Mechanics and Engineering*, vol. 199, n. 45, pp. 2765–2778.
[3] Miehe, C., Hofacker, M., Schänzel, L.-M., & Aldakheel, F., 2015. Phase field modeling of fracture in multi-physics problems. part ii. coupled brittle-to-ductile failure criteria and crack propagation in thermo-elastic–plastic solids. *Computer Methods in Applied Mechanics and Engineering*, vol. 294, pp. 486–522.
[4] Ambati, M., Gerasimov, T., & De Lorenzis, L., 2015. Phase-field modeling of ductile fracture. *Computational Mechanics*, vol. 55, n. 5, pp. 1017–1040.
[5] Ambati, M. & De Lorenzis, L., 2016. Phase-field modeling of brittle and ductile fracture in shells with isogeometric nurbs-based solid-shell elements. *Computer Methods in Applied Mechanics and Engineering*, vol. 312, pp. 351–373.
[6] Borden, M. J., Hughes, T. J., Landis, C. M., Anvari, A., & Lee, I. J., 2016. A phase-field formulation for fracture in ductile materials: Finite deformation balance law derivation, plastic degradation, and stress triaxiality effects. *Computer Methods in Applied Mechanics and Engineering*, vol. 312, pp. 130–166.
[7] Haveroth, G., Vale, M., Bittencourt, M., & Boldrini, J., 2020. A non-isothermal thermodynamically consistent phase field model for damage, fracture and fatigue evolutions in elasto-plastic materials. *Computer Methods in Applied Mechanics and Engineering*, vol. 364, pp. 112962.
[8] Nguyen, T.-T., Yvonnet, J., Zhu, Q.-Z., Bornert, M., & Chateau, C., 2016. A phase-field method for computational modeling of interfacial damage interacting with crack propagation in realistic microstructures obtained by microtomography. *Computer Methods in Applied Mechanics and Engineering*, vol. 312, pp. 567–595.
[9] Miehe, C., Welschinger, F., & Hofacker, M., 2010b. Thermodynamically consistent phase-field models of fracture: variational principles and multi-field FE implementations. *International Journal for Numerical Methods in Engineering*, vol. 83, n. 10, pp. 1273–1311.
[10] Borden, M. J., Verhoosel, C. V., Scott, M. A., Hughes, T. J., & Landis, C. M., 2012. A phase-field description of dynamic brittle fracture. *Computer Methods in Applied Mechanics and Engineering*, vol. 217, pp. 77–95.
[11] Borden, M. J., Hughes, T. J., Landis, C. M., & Verhoosel, C. V., 2014. A higher-order phase-field model for brittle fracture: Formulation and analysis within the isogeometric analysis framework. *Computer Methods in Applied Mechanics and Engineering*, vol. 273, pp. 100–118.
[12] Ulmer, H., Hofacker, M., & Miehe, C., 2013. Phase field modeling of brittle and ductile fracture. *PAMM*, vol. 13, n. 1, pp. 533–536.
[13] Ambati, M., Kruse, R., & De Lorenzis, L., 2016. A phase-field model for ductile fracture at finite strains and its experimental verification. *Computational Mechanics*, vol. 57, n. 1, pp. 149–167.
[14] Leeper, F. E. J. & Allen, S. E. R., 2015. *Guidelines to Best Practices For Heavy Haul Railway Operations: Management of the Wheel and Rail*, volume 3. International Heavy Haul Association (IHHA), Virginia, USA, second edition.
[15] Tan, W., Falzon, B. G., Chiu, L. N. S., & Price, M., 2015. Predicting low velocity impact damage and compression-after-impact (cai) behaviour of composite laminates. *Composites Part A: Applied Science and Manufacturing*, vol. 71, pp. 212 – 226.
[16] Yan, H., Oskay, C., Krishnan, A., & Xu, L. R., 2010. Compression-after-impact response of woven fiber-reinforced composites. *Composites Science and Technology*, vol. 70, n. 14, pp. 2128 – 2136.
[17] Camacho, G. T. & Ortiz, M., 1996. Computational modelling of impact damage in brittle materials. *International Journal of Solids and Structures*, vol. 33, n. 20, pp. 2899 – 2938.
[18] Körbelin, J., Derra, M., & Fiedler, B., 2018. Influence of temperature and impact energy on low velocity impact damage severity in cfrp. *Composites Part A: Applied Science and Manufacturing*, vol. 115, pp. 76 – 87.
[19] Franke, M., Hesch, C., & Dittmann, M., 2016. Phase-field approach to fracture for finite-deformation contact problems. *PAMM*, vol. 16, n. 1, pp. 123–124.
[20] Hesch, C., Franke, M., Dittmann, M., & Temizer, I., 2016. Hierarchical nurbs and a higher-order phase-field approach to fracture for finite-deformation contact problems. *Computer Methods in Applied Mechanics and Engineering*, vol. 301, pp. 242–258.
[21] Wriggers, P. & Zavarise, G., 2004. Computational contact mechanics. *Encyclopedia of computational mechanics*.
[22] Fabrizio, M., Giorgi, C., & Morro, A., 2006. A thermodynamic approach to non-isothermal phase-field evolution in continuum physics. *Physica D: Nonlinear Phenomena*, vol. 214, n. 2, pp. 144–156.

[23] Frémond, M., 2013. *Non-smooth thermomechanics*. Springer Science & Business Media.
[24] Simo, J. C., 1988. A framework for finite strain elastoplasticity based on maximum plastic dissipation and the multiplicative decomposition: Part i. continuum formulation. *Computer methods in applied mechanics and engineering*, vol. 66, n. 2, pp. 199–219.
[25] Haveroth, G. A., 2020. *Phase field models for problems involving fracture, plasticity and finite strains*. University of Campinas.
[26] Lu, S. & Pister, K., 1975. Decomposition of deformation and representation of the free energy function for isotropic thermoelastic solids. *International Journal of Solids and Structures*, vol. 11, n. 7-8, pp. 927–934.
[27] Miehe, C., 1988. *Zur numerischen Behandlung thermomechanischer Prozesse*. PhD thesis, Institut für Baumechanik und Numerische Mechanik, Universität Hannover, Hannover.
[28] Simo, J. C. & Hughes, T. J. R., 1998. *Computational Inelasticity*. Springer-Verlag.
[29] Jain, M., Lloyd, D., & Macewen, S., 1996. Hardening laws, surface roughness and biaxial tensile limit strains of sheet aluminium alloys. *International journal of mechanical sciences*, vol. 38, n. 2, pp. 219–232.
[30] Laursen, T. A., 2013. *Computational contact and impact mechanics: fundamentals of modeling interfacial phenomena in nonlinear finite element analysis*. Springer Science & Business Media.
[31] Dias, A. P. C., 2017. *Numerical Simulation of Structural Contact Problems with High-Order Mortar-Based Element*. PhD thesis, Department of Integrated Systems, School of Mechanical Engineering, University of Campinas, Campinas - Brazil.
[32] Fischer, K. A. & Wriggers, P., 2006. Mortar based frictional contact formulation for higher order interpolations using the moving friction cone. *Computer methods in applied mechanics and engineering*, vol. 195, n. 37-40, pp. 5020–5036.
[33] Wriggers, P. & Haraldsson, A., 2003. A simple formulation for two-dimensional contact problems using a moving friction cone. *Communications in numerical methods in engineering*, vol. 19, n. 4, pp. 285–295.
[34] Wriggers, P., 2003. Computational contact mechanics. *Computational Mechanics*, vol. 32, n. 1, pp. 141–141.
[35] Luenberger, D. G., Ye, Y., et al., 1984. *Linear and nonlinear programming*, volume 2. Springer.
[36] Dias, A. P. C., Serpa, A. L., & Bittencourt, M. L., 2015. High-order mortar-based element applied to nonlinear analysis of structural contact mechanics. *Computer Methods in Applied Mechanics and Engineering*, vol. 294, pp. 19–55.
[37] Dias, A. P. C., Proenca, S. P. B., & Bittencourt, M. L., 2018a. *Advances in Computational Coupling and Contact Mechanics: Chapter 2-Standard and Generalized High-order Mortar-based Finite Elements in Computational Contact Mechanics*, volume 1. World Scientific (EUROPE), London, UK, first edition.
[38] Dias, A. P. C., Proenca, S. P. B., & Bittencourt, M. L., 2018b. High-order mortar-based contact element using NURBS for the mapping of contact curved surfaces. *Computational Mechanics - https://doi.org/10.1007/s00466-018-1658-6*.
[39] Bhatti, M. A., 2006. *Advanced topics in finite element analysis of structures: with Mathematica and MATLAB computations*. John Wiley & Sons, Inc.